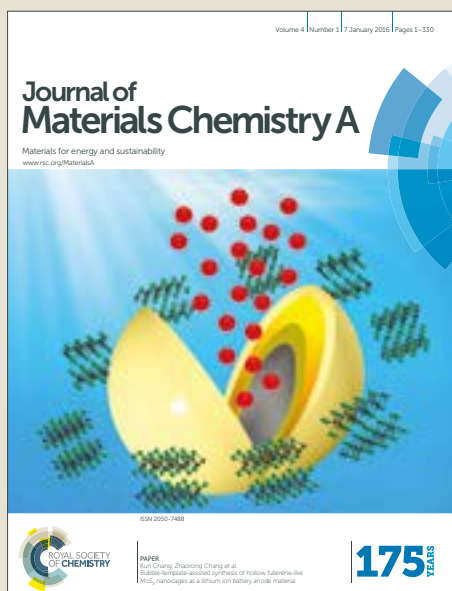


Journal of Materials Chemistry A

Accepted Manuscript



This article can be cited before page numbers have been issued, to do this please use: K. Wang, L. Zhang, Y. Su, D. Shao, S. Zeng and W. Wang, *J. Mater. Chem. A*, 2018, DOI: 10.1039/C8TA01309H.



This is an Accepted Manuscript, which has been through the Royal Society of Chemistry peer review process and has been accepted for publication.

Accepted Manuscripts are published online shortly after acceptance, before technical editing, formatting and proof reading. Using this free service, authors can make their results available to the community, in citable form, before we publish the edited article. We will replace this Accepted Manuscript with the edited and formatted Advance Article as soon as it is available.

You can find more information about Accepted Manuscripts in the [author guidelines](#).

Please note that technical editing may introduce minor changes to the text and/or graphics, which may alter content. The journal's standard [Terms & Conditions](#) and the ethical guidelines, outlined in our [author and reviewer resource centre](#), still apply. In no event shall the Royal Society of Chemistry be held responsible for any errors or omissions in this Accepted Manuscript or any consequences arising from the use of any information it contains.

Photoreduction of carbon dioxide of atmospheric concentration with water to methane over CoAl-Layered Double Hydroxide nanosheets†

Received 00th January 20xx,
Accepted 00th January 20xx

DOI: 10.1039/x0xx00000x

www.rsc.org/

Kefu Wang,^{ab} Ling Zhang,^a Yang Su,^{ab} Dengkui Shao,^{ab} Shuwen Zeng,^{ab} Wenzhong Wang^{*a}

Photoreduction of CO₂ to carbon energy resources over catalysts is of great interest and significance. However, many works are conducted under high CO₂ concentration, research on CO₂ photoreduction under atmospheric concentration remains rare. Here, CoAl-Layered Double Hydroxide (CoAl-LDH) nanosheets have been synthesized as a platform to explore low-concentration CO₂ photoreduction. The CoAl-LDH nanosheets exhibit efficient photocatalytic activity for CO₂ photoreduction of atmospheric concentration (400 ppm) to CH₄ under simulated solar light and proceed without deactivation after 55 hours. A CH₄ production rate of 4.3 μmol·g⁻¹·h⁻¹ is achieved without the assistant of any sacrificial agent or noble metal. CO₂ adsorption experiments show that CoAl-LDH nanosheets exhibit an adsorption capacity of 2.95 cm³·g⁻¹, which is about two times than that of P25 with a comparative specific surface area. XPS analysis indicates that CH₄ generation relates closely to the divalent cobalt and the CH₄ yield decreases sharply when the divalent cobalt is oxidized, which could likely be ascribed to the divalent cobalt for dissociating water to release H for hydrogenation of the intermediates through further experimental analysis. This work emphasizes the importance of alkaline OH group for the efficient adsorption of low-concentration CO₂ and reveals the unique property of the divalent cobalt for CO₂ photoreduction.

1. Introduction

The atmospheric CO₂ concentration has been monotonically growing with the increasing consumption of fossil fuels, bringing about adverse environmental issue, and the overusing of fossil fuels could lead to greater energy shortage ulteriorly.¹ Artificial photosynthesis, which utilizes semiconductor photocatalysts to convert CO₂ and water into substances of energy sources (such as CO, CH₃OH, CH₄), is possibly one of the most sustainable and ideal solutions to simultaneously address the problems of the global warming and energy crisis.² However, CO₂ is pretty stable with a high dissociation energy of ~750 kJ mol⁻¹ for C=O bond under normal conditions.³ In addition, the photoreduction of CO₂ is a multi-electron process and usually involves the activation of water, which has not been commendably resolved at the moment. Searching for an efficient photocatalyst with multi-function seems to be necessary to meet the challenge. Up till now, various photocatalysts for efficient CO₂ reduction have been reported,⁴⁻

¹⁵ while most of these research is implemented under CO₂ atmosphere with high concentration. Converting CO₂ of atmospheric concentration into carbon energy sources is rare and deserves to be explored in view of the low concentration of CO₂ in the atmosphere. Besides, the primary products of CO₂ photoreduction are CO or HCOOH, and a high selectivity for CH₄ product remains difficult, possibly hindered by the further conversion of intermediates. Improving the CO₂ adsorption and promoting hydrogenation process of the intermediates seem to be the key to solve the problem.

In consideration of the Lewis acidity of CO₂, alkaline catalysts will benefit the adsorption and activation of CO₂. Surface modification of TiO₂ with NaOH has been reported to greatly promote the photoreduction of CO₂ to CH₄, which is considered to derive from efficient chemisorption and activation by forming carbonate species.⁴ Moreover, artificial photosynthesis contains the processes of CO₂ reduction and H₂O oxidation simultaneously, demanding the photocatalysts dual functions. Recently, layered materials have attracted much attention.¹⁶ Layered materials usually possess high specific surface area, meaning affluent active sites for catalytic reaction. Among the layered materials, layered double hydroxides (LDHs) are common but important photocatalysts, with their host structure based on brucite-like layers with edge-sharing MO₆ octahedra. Edge-sharing MO₆ octahedra units result in the formation of 2D sheets, in which the metal cations are six-fold coordinated by OH groups.¹⁷ It is proposed that the alkaline OH groups of layered double hydroxides are in favor of the adsorption of CO₂ and may also help to activate CO₂ molecules. Besides, LDHs have been reported to be efficient photocatalysts

^a State Key Laboratory of High Performance Ceramics and Super fine Microstructure, Shanghai Institute of Ceramics, Chinese Academy of Sciences, 1295 Dingxi Road, Shanghai 200050, P. R. China.

^b University of Chinese Academy of Sciences, Beijing 100049, P.R. China.

*E-mail: wzwang@mail.sic.ac.cn

† Electronic Supplementary Information (ESI) available: EDS and EDS mapping, UV-visible absorption spectrum, Blank experiments, CO and H₂ evolution of CoAl-LDH nanosheets. CH₄ evolution of CoAl-LDH and P25. Summary of the activities of some widely used semiconductor catalysts. XRD patterns of CoAl-n (n=0, 0.25, 0.5, 2). CO₂ adsorption capacities of CoAl-n (n=0, 2) and some other kinds of LDH. XRD patterns, UV-visible absorption spectra, FT-IR spectra and CH₄ evolution of some other LDHs. See DOI: 10.1039/x0xx00000x

for water oxidation.¹⁸⁻²¹ It is expected that LDHs might possess the dual properties of CO₂ activation and H₂O oxidation. Hence, LDHs could be desired catalysts for CO₂ photoreduction.

In this work, CoAl-LDH nanosheets were synthesized. They were found to be active and stable in the photoreduction of CO₂ to CH₄ without obvious deactivation even after 55 hours. The CH₄ production rate of 4.3 μmol·g⁻¹·h⁻¹ was achieved under atmospheric CO₂ concentration (about 400 ppm) without the assistance of any sacrificial agent or noble metal. The good performance could likely be attributed to the surface alkaline OH groups for efficient adsorption of low-concentration CO₂ and the divalent cobalt for the unique and effective electronic structure configuration, which could be demonstrated that the catalytic efficiency decreased sharply when the divalent cobalt was oxidized. Further experimental study indicated that the divalent cobalt oxidized might lose the ability to dissociate water and no hydrogen was released for the hydrogenation process of the intermediate products.

2. Experimental

2.1 Catalyst preparation

All reagents were of analytical purity and received from Shanghai Chemical Company without further purification. CoAl-LDH nanosheets were synthesized in a simple co-precipitation method. Typically, cobalt nitrate hexahydrate (0.582 g, 2 mmol) and aluminum nitrate nonahydrate (0.375 g, 1 mmol) were dissolved in de-ionized water (20 mL) (noted as solution A). Stirring the solution for 15 min. Sodium hydroxide (0.24 g, 6 mmol) and anhydrous sodium carbonate (0.053 g, 0.5 mmol) were dissolved in deionized water (20 mL) with stirring (noted as solution B). Then solution A was added dropwise into solution B and the suspension was transferred to a Teflon-lined autoclave (50 mL), sealed and heated at 110 °C for 9 h. The products were filtered and washed thoroughly with de-ionized water and dried in vacuum oven at 60 °C.

2.2 Materials characterization

The crystallinity of the as-prepared catalyst samples was characterized by powder X-ray diffraction (XRD) with a Rigaku D/MAX 2250 V diffractometer using monochromatized Cu Kα (λ = 0.15418 nm) radiation while the voltage and electric current were held at 40 kV and 100 mA. The morphologies and microstructures characterizations were performed on the transmission electron microscope (TEM, JEOL JEM-2100F, accelerating voltage 200 kV). UV-Vis diffuse reflectance spectra (DRS) of the samples were obtained on an UV-Vis spectrophotometer (Hitachi U-3010). X-ray photoelectron spectroscopy (XPS) was performed on an ESCALAB 250, Thermo Scientific Ltd. with a 320 μm diameter spot of monochromated aluminum Kα X-rays at 1486.6 eV under ultrahigh-vacuum conditions. FTIR spectra presented in this work were recorded on a Bruker Tensor 27 spectrometer. In situ infrared spectra presented in this work were recorded on a NICOLET iS10 apparatus with a cavity (about 20 cm³) for adjusting atmosphere. The Raman spectra were recorded on a Horiba

LABRAM HR, with a 532 nm excitation laser line. Brunauer-Emmett-Teller (BET) specific surface area and Barrett-Joyner-Halenda (BJH) pore size distribution were measured by a surface area and pore size analyzer (V-sorb 2008 P, Gold APP).

2.3 Photocatalytic reactions

The experiments of gas-phase CO₂ photoreduction with H₂O on CoAl-LDH nanosheets were carried out in a closed pyrex cell (600 mL) with a quartz window. First, CoAl-LDH powder (30 mg) was sprinkled on bottom of the pyrex cell. Water (0.5 mL) was then sprayed around the catalyst. Prior to the irradiation of a Xe lamp (500 W), the cell was purged with dry nitrogen, followed by injection of CO₂ (0.25 mL, about 400 ppm). The gaseous products (CO, CH₄) were analyzed by a gas chromatograph (GC, Tianmei 7890) equipped with a flame ionization detector (FID). The H₂ product was analyzed by a GC (Tianmei 7890II) equipped with a thermal conductivity detector (TCD).

2.4 Electrochemical measurements

The electrochemical analysis was performed on a CHI 660D electrochemical workstation (Shanghai Chenhua, China) using a standard three-electrode quartz cell with a working electrode, a platinum slice as the counter electrode, and a standard saturated calomel electrode (SCE) in saturated KCl as the reference electrode. To make a working electrode, catalyst powders were deposited on a fluorine-doped tin oxide (FTO) substrate by coating. Briefly, 10 mg of catalyst was suspended in 1 mL ethanol solution and the mixtures were ultrasonically scattered for 15 min. Then, 100 μL of above slurry was coated on the FTO glass. After natural evaporation of ethanol, the catalyst coated on FTO substrate was used as the working electrode. The area (S) for the coating layer is about 0.8 cm², while the thickness (L) is about 0.02 cm. The electrical resistivity (ρ) is calculated by $\rho = R \cdot S / L$, where R could be measured by the electrochemical impedance spectroscopy (EIS). During the measurements, the electrolyte of 0.1 M Na₂SO₄ solution (pH = 7) was utilized.

2.5 CO₂ adsorption measurements

In order to accurately characterize the CO₂ adsorption capacity of catalysts under the experimental environment, CO₂ adsorption measurements were conducted in a closed pyrex cell (600 mL). Typically, the cell was purged with dry nitrogen for half an hour, followed by injection of CO₂ (0.25 mL), then the CO₂ concentration was detected (noted as N₀) by gas chromatograph to obtain the ratio K between the amount of CO₂ and the CO₂ concentration (The detected CO₂ concentration by gas chromatograph keeps a linear relationship with the amount of injected CO₂). Control experiments were conducted when catalysts (30 mg) were sprinkled on bottom of the pyrex cell, followed by injection of CO₂ (0.25 mL), then the CO₂ concentration was detected (noted as N₁). The CO₂ adsorption capacity could be obtained by the formula $A = (N_0 - N_1) \cdot K$. The experiments were repeated for three times to ensure the veracity.

3. Results and discussion

3.1 Structure and morphology

CoAl-LDH nanosheets have been prepared by a simple co-precipitation method. TEM images (Figure 1A-C) show that the CoAl-LDHs possess a hexagonal sheet-like morphology with a lateral size of about 80 nm and a thickness of about 18 nm. From the SAED pattern in Figure 1D, hexagonally arranged spots are observed and the corresponding spots could be allotted to (012) and (110) planes of CoAl-LDH. The EDS profile of CoAl-LDH nanosheets (Figure S1) indicates the presence of Co, Al, O elements, and the elemental mapping exhibits a relatively uniform distribution of these constituent elements.

Powder XRD data (Figure 2A) shows the product to be a typical rhombohedral structure with the lattice parameters of $a=b=0.306$ nm and $c=2.263$ nm ($a=b=2d_{110}$, $c=3d_{003}$).²² The Bragg reflections in the XRD could be indexed as (003), (006), (012), (110), (113) and (116), respectively, which are consistent with those of well-known LDH materials.²³ To analysis the surface and interior structure of CoAl-LDH nanosheets, FT-IR spectra and Raman spectra were exploited. As shown in Figure 2B, the broad strong absorption band around 3430 cm^{-1} is attributed to the stretching vibrations of surface hydroxyl groups and interlayer water molecules, indicating that hydrogen bonds with a wide range of strength existed, while the weak band centered at 1628 cm^{-1} is due to the bending mode of water.²⁴ The absorption band at 1358 cm^{-1} , 1038 cm^{-1} , 808 cm^{-1} could be assigned to ν_3 mode (asymmetric stretching), ν_1 mode (symmetric stretching), ν_2 mode (out-of-plane deformation) of the carbonate, respectively.^{25,26} Although the ν_1 mode is IR-inactive in the free carbonate, it becomes activated owing to the lowering of symmetry of carbonate anion in the interlayer.²⁶ The band remained in the low-frequency region could be interpreted as the lattice vibration modes, such as 617 cm^{-1} , 547 cm^{-1} , 427 cm^{-1} corresponding to the Co-OH stretching, O-Co-O stretching, Al-OH stretching, respectively.^{24,25} As for the Raman spectra (Figure 2C), the broad band around 3480 cm^{-1} is attributed to the H-banded stretching vibrations of hydroxyl

groups of the brucite-like sheets, analogous to the infrared spectra. The sharp band at 1056 cm^{-1} is assigned to in-plane OH bending vibrations, with a second band at a slightly lower Raman shift of 1044 cm^{-1} assigned to ν_1 mode of the carbonate.²⁵ With regard to the low frequency region lower than 1000 cm^{-1} , the bands at 545 cm^{-1} and 508 cm^{-1} stems from Al-OH vibrations, while the band centered at 153 cm^{-1} could be due to the framework vibrations.²⁷

The specific surface area and porosity property of the CoAl-LDH nanosheets were studied by nitrogen Brunauer-Emmett-Teller (Figure 2D), which shows a type IV isotherm with H3 hysteresis loop, indicating the presence of mesopores. The sample illustrates a wide pore-size distribution in the range of 2-200 nm and a high surface area of 37.7 m^2g^{-1} . The high specific surface area of CoAl-LDH nanosheets is expected to be in favor of CO_2 uptake and to provide more active sites, so as to improve the photocatalytic activity.

The UV-visible absorption spectrum of CoAl-LDH nanosheets is displayed in Figure S2. The absorption peak around 500 nm corresponds to the $4T_{1g}(F) \rightarrow 4T_{1g}(P)$ transition of Co^{2+} octahedrally coordinated by weak-field ligands, while the peak around 600 nm could be due to the $3A_{2g}(F) \rightarrow 3T_{1g}(F)$ transition arising from spin-orbit coupling.²⁸ The UV absorption around 230 nm may stem from ligand to metal charge transfer within the CoAl-LDH layer. The associated Tauc plot (Figure 3A) reveals that the optical band gap for CoAl-LDH nanosheets is 2.1 eV.^{15,21} To determine the positions of band edge related to redox potentials of CO_2 photoreduction, electrochemical experiment for Mott-Schottky plot was performed to measure the flat-band potential (E_{fb}) of CoAl-LDHs. As shown in Figure 3B, the negative slope of the plot indicates that CoAl-LDH is a characteristic p-type semiconductor. The E_{fb} of CoAl-LDH measured from the intercept of the axis with potential value is 0.66 V vs NHE (0.42 V vs SCE) at pH 7. Generally, the position of E_{fb} is considered to be about 0.3 V above the top of the valence band (E_{vb}) for the p-type semiconductor whose electrical resistivity is in the range of $10^3 - 10^4$ $\Omega\text{-cm}$, while the electrical resistivity of CoAl-LDH is

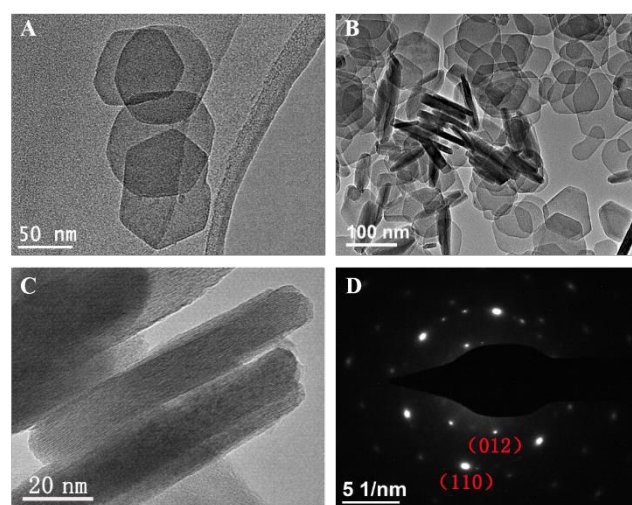


Figure 1. (A-C) TEM images and (D) SAED pattern of CoAl-LDH nanosheets.

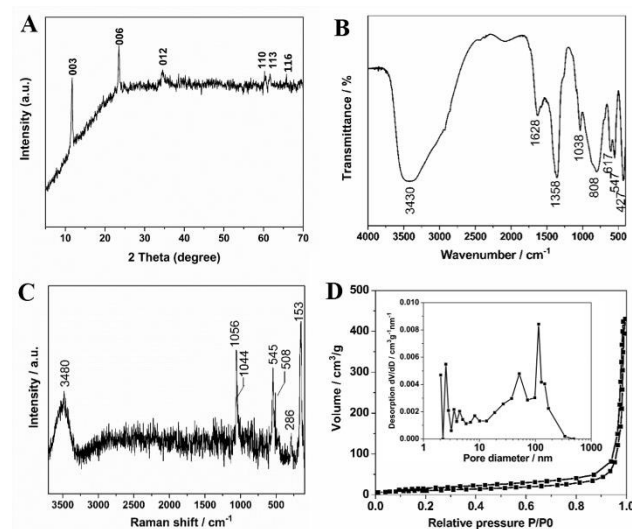


Figure 2. (A) XRD pattern, (B) FT-IR spectrum, (C) Raman spectrum, (D) N_2 adsorption-desorption isotherm and pore size distribution of CoAl-LDH nanosheets.

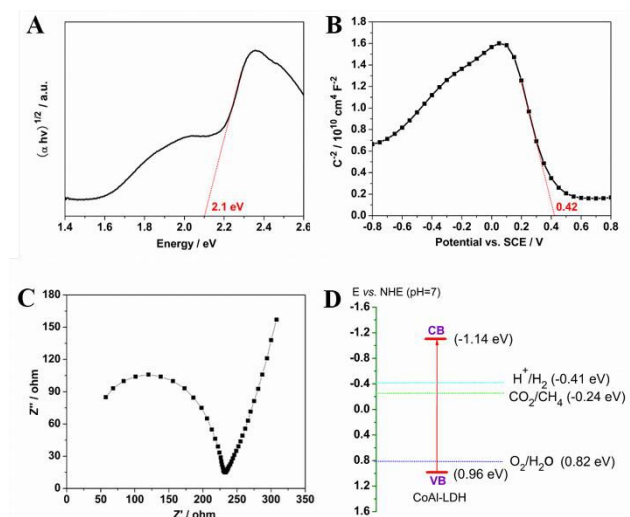


Figure 3. (A) Tauc plot of CoAl-LDH nanosheets. (B) Mott-Schottky plot of CoAl-LDH nanosheets. (C) Electrochemical impedance spectroscopy of CoAl-LDH nanosheets. (D) Band structure of CoAl-LDH nanosheets.

calculated to be about $9 \times 10^3 \Omega \cdot \text{cm}$ (Figure 3C, $\rho = R \cdot S / L$, $R \approx 230 \Omega$, $S = 0.8 \text{ cm}^2$, $L = 0.02 \text{ cm}$).^{29,30} Therefore, the E_{vb} of CoAl-LDH is supposed to be 0.96 V vs NHE, and the corresponding conduction band (E_{cb}) is then calculated to be about -1.14 eV vs NHE according to the band gap (2.1 eV). As can be seen in Figure 3D, the positions of the conduction band edge and the valence band edge sit astride the redox potentials of CO_2 reduction and water oxidation, indicating the feasibility of CO_2 photoreduction for CoAl-LDH nanosheets.

3.2 Photocatalytic activity

To exclude the possible influence of environmental contaminations on photocatalysts and the reaction equipment, photocatalysts in closed pyrex cell were first illuminated for three hours without injecting water and CO_2 to affirm no CO and CH_4 product was released before measuring photocatalytic activity. Blank experiment was conducted with CoAl-LDH nanosheets in the absence of CO_2 under photoillumination. Neither CO nor CH_4 was detected, confirming CO_2 was indeed the carbon source (Figure S3, S4). Another control experiment was done without either illumination or CoAl-LDH nanosheets, no products were detected, indicating that both the light irradiation and CoAl-LDH nanosheets were necessary for CO_2 photoreduction. The predominant reaction product was CH_4 , whose yield as a function of irradiation time is plotted in Figure

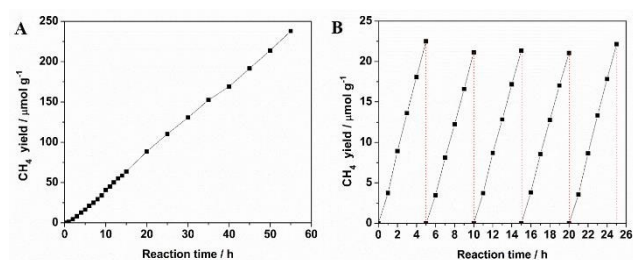


Figure 4. (A) Time course of CH_4 evolution for CoAl-LDH nanosheets in the photocatalytic conversion of CO_2 with water. (B) Cycling curves of photocatalytic production of CH_4 on CoAl-LDH nanosheets.

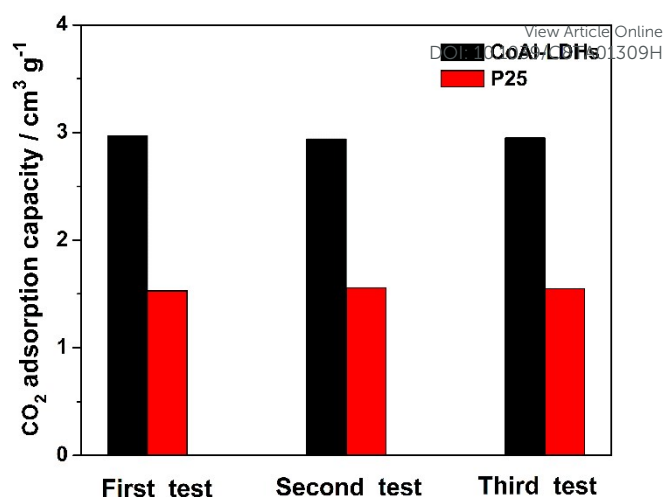


Figure 5. CO_2 adsorption measurements of CoAl-LDHs and P25 for three times.

Table 1. CO_2 adsorption capacities of CoAl-LDHs and P25 for three times.

Sample	First test	Second test	Third test	Average ($\text{cm}^3 \text{ g}^{-1}$)	Standard deviation ($\text{cm}^3 \text{ g}^{-1}$)
CoAl-LDHs	2.97	2.94	2.95	2.95	0.0129
P25	1.53	1.57	1.55	1.55	0.0163

4A. Meanwhile, a small amount of CO and H_2 were also detected (Figure S5). Interestingly, the yield of CO and H_2 became balanced after several hours of reaction and did not increase anymore, which might indicate that it reached an equilibrium between the production rate and consumption rate. The CH_4 yield gradually increased with the reaction time and reached an overall value of $238 \mu\text{mol} \cdot \text{g}^{-1}$ in 55 hours (corresponding to approximately $4.3 \mu\text{mol} \cdot \text{g}^{-1} \cdot \text{h}^{-1}$), which was efficient for a pure semiconductor without any modifications, and the average CH_4 formation rate of CoAl-LDH nanosheets ($4.2 \mu\text{mol} \cdot \text{g}^{-1} \cdot \text{h}^{-1}$) was 13 times higher than that of P25 ($0.3 \mu\text{mol} \cdot \text{g}^{-1} \cdot \text{h}^{-1}$) for five hours' reaction (Figure S6, supporting information). The CH_4 selectivity for CO_2 conversion reached 92% (selectivity = $N_{\text{CH}_4} / N_{(\text{CH}_4 + \text{CO})} \cdot 100\%$) in 55 hours, while the CH_4 selectivity for whole reduction products was calculated to be 77% (selectivity = $N_{\text{CH}_4} / N_{(\text{CH}_4 + \text{CO} + \text{H}_2)} \cdot 100\%$). Table S1 (supporting information) summarizes the activities of some widely used semiconductor catalysts. It can be seen that CoAl-LDH nanosheets are of high efficiency for the photoreduction of CO_2 to CH_4 . More importantly, the CO_2 photoreduction activity did not show any significant loss even after 55 hours, indicating the good photostability of CoAl-LDH nanosheets. Besides, CoAl-LDH nanosheets were conducted for five cycles of repetition test (Figure 4B), the CH_4 generation rate remained almost unchanged, which confirms the stability further.

3.3 Mechanism and discussion

So the question is why the CoAl-LDH nanosheets exhibited high activity for photoreduction of CO_2 to CH_4 under low-concentration CO_2 atmosphere. The origins are considered to

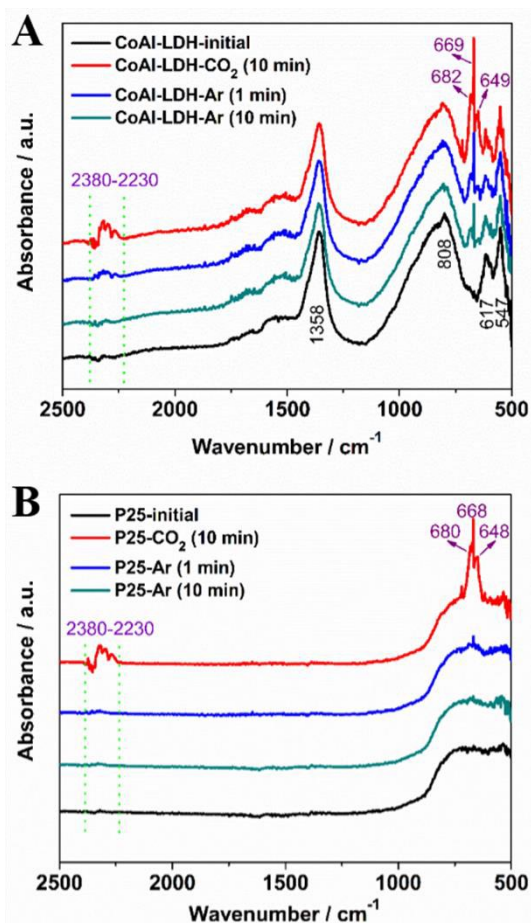


Figure 6. (A) In situ FT-IR spectra for CO₂ adsorption on CoAl-LDHs. (B) In situ FT-IR spectra for CO₂ adsorption on P25.

derive from the surface alkaline OH groups for efficient adsorption of low-concentration CO₂ and the divalent cobalt for dissociating water to release hydrogen for the hydrogenation process of the intermediates, which will be discussed in detail in this section.

3.31. Efficient adsorption of CO₂

To accurately present the CO₂ adsorbing capacity of the catalysts in the experimental environment, CO₂ adsorption measurements were conducted in the closed pyrex cell used for photocatalytic reaction. As shown in Figure 5, CoAl-LDHs exhibited an admirable adsorption capacity of 2.95 cm³·g⁻¹, which was about two times than that of P25 (1.55 cm³·g⁻¹) with a comparative specific surface area (50 m²·g⁻¹), indicating the efficient adsorption of low-concentration CO₂ for CoAl-LDHs. The experiments were repeated for three times to ensure the veracity. Table 1 shows that the measured values kept almost the same, and the standard deviation of CO₂ adsorption capacity was much smaller than the CO₂ adsorption capacity, manifesting the reliability of the experimental method. In addition, some other LDHs were conducted on CO₂ adsorption experiments as well, and all of them exhibited good adsorption of CO₂ molecules (Figure S7), probably due to the surface OH groups.

In situ FT-IR spectra were implemented to investigate CO₂

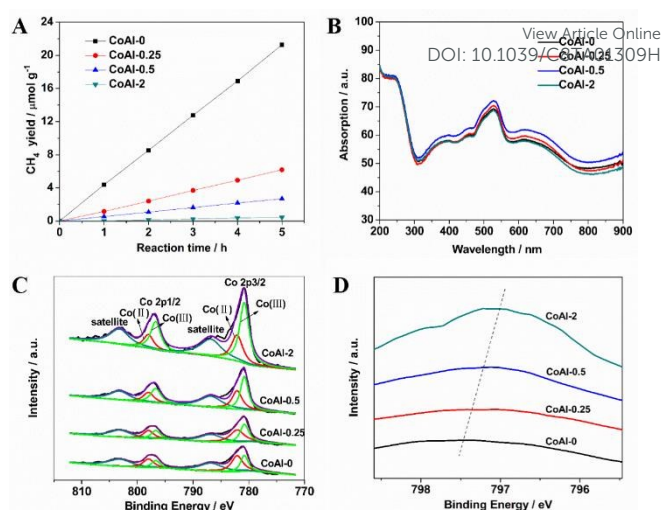


Figure 7. (A) Time course of CH₄ evolution for CoAl-n (n=0, 0.25, 0.5, 2). (B) DRS spectra of CoAl-n (n=0, 0.25, 0.5, 2). (C) XPS spectra of the Co 2p region for CoAl-n (n=0, 0.25, 0.5, 2). (D) The magnified XPS spectra of Co 2p_{1/2} region for CoAl-n (n=0, 0.25, 0.5, 2).

adsorption further. First, the spectrum for CoAl-LDHs (noted as CoAl-LDH-initial) was recorded when the apparatus was purged with dry argon. Dry CO₂ was then introduced for 10 min (20 mL/min) and the spectrum was recorded (noted as CoAl-LDH-CO₂ (10 min)). Argon was subsequently used to expel the CO₂ for 1 min, 10 min (20 mL/min, noted as CoAl-LDH-Ar (1 min) and CoAl-LDH-Ar (10 min), respectively). As shown in Figure 6A, several absorption bands at 2230-2380 cm⁻¹ appeared after the introduction of CO₂, which are typical of the ν₃ anti-symmetric stretching modes of CO₂ gas, while the new-emerging bands at 682 cm⁻¹, 669 cm⁻¹ and 649 cm⁻¹ could be attributed to the splitting of the ν₂ bending mode of adsorbed CO₂.^{31,32} After the expelling of CO₂ by argon, it was observed that the absorption bands at 2230-2380 cm⁻¹ became weakened and vanished at last, indicating that CO₂ gas was nearly expelled. However, we could find that the bands around 669 cm⁻¹ remained and had not been blown away, revealing a good adsorption of CO₂. With regard to the spectra for P25 (Figure 6B), similar absorption bands were observed after the introduction of CO₂. Nevertheless, the bands decreased rapidly and vanished at last after expelling by argon. Therefore, it is proposed that the efficient adsorption of CO₂ for CoAl-LDHs could contribute to CO₂ photoreduction.

3.32. Divalent cobalt for the unique and effective property

Further experiments have been conducted to demonstrate the unique effect of the divalent cobalt in CoAl-LDHs for CO₂ photoreduction to CH₄. The divalent cobalt was oxidized by heating the CoAl-LDHs in oxygen atmosphere at 85 °C for 0 h, 0.25 h, 0.5 h, 2 h (donated as CoAl-0, CoAl-0.25, CoAl-0.5, CoAl-2), respectively. It is expected that cobalt (II) would be oxidized to cobalt (III) and a series of CoAl-LDHs with different cobalt (II) concentrations were prepared.³³ As shown in Figure 7A, the catalytic activity for CO₂ photoreduction to CH₄ decreased sharply with the oxidation time of CoAl-LDHs increasing, while there was no significant difference between CoAl-n (n=0, 0.25, 0.5, 2) samples in the X-ray diffraction (Figure S8), indicating

that the phase change of CoAl-LDHs had not occurred during the oxidation for different time, which could also be confirmed by the UV-visible diffuse reflectance spectra. The DRS spectra of CoAl-*n* (*n*=0, 0.25, 0.5, 2) did not show much difference (Figure 7B). XPS analysis was then carried out to obtain the surface information of the samples. As shown in Figure 7C, the two strong peaks in the Co region around 797.3 eV and 781.4 eV could be assigned to Co 2p_{1/2} and Co 2p_{3/2}, while the other two peaks around 803.7 eV and 787.5 eV could be assigned to the satellite peaks of Co 2p_{1/2} and Co 2p_{3/2}, respectively.³⁴ Generally, the peaks at 798 eV and 797 eV in Co 2p_{1/2} band were severally indicative of cobalt (II) and cobalt (III).³⁵⁻³⁸ On account of the oxidation of divalent cobalt for different times, it was found that the peak position of Co 2p_{1/2} had moved to lower binding energy with the prolongation of oxidation time (Figure 7D), indicating that the oxidation degree of divalent cobalt improved from CoAl-0 to CoAl-2 (CoAl-*n*, *n*=0, 0.25, 0.5, 2). Figure 7C also shows that the ratio between cobalt (II) and cobalt (III) decreased when extending the oxidation time. All these above make it clear that CoAl-*n* (*n*=0, 0.25, 0.5, 2) just distinguished from each other with the oxidation degree of divalent cobalt on the surface, but with bulk phase to be the same. However, CoAl-*n* (*n*=0, 0.25, 0.5, 2) differed greatly on the activity of CO₂ photoreduction, and it does not take much effort to find that the catalytic activity of CO₂ photoreduction to CH₄ decreased sharply with the oxidation degree of divalent cobalt increasing, which strongly confirms that the divalent Cobalt plays a key role in CH₄ generation.

CO₂ adsorption experiments showed that the CO₂ adsorbing capacity of CoAl-*n* (*n*=0, 2) remained almost unchanged (Figure S9), declaring that the decrease of catalytic activity had no relation with the CO₂ adsorption. To gain deeper insights into the reason for the poor photocatalytic activity of CoAl-LDHs once the divalent cobalt was oxidized, some traces were seized through other products (such as CO, H₂) for CO₂ photoreduction. CO or HCOOH is generally considered to be the primary intermediate for CO₂ photoreduction to CH₄.³⁹ In this reaction system of CoAl-LDHs, CO was expected to be the primary intermediate in view of that abundant CO was generated and could be further consumed as the reactant. If a large amount of HCOOH was produced as the primary intermediate, CoAl-LDH catalyst would be gradually corroded with reaction time. However, CoAl-LDHs were of good stability in photocatalytic process.

CoAl-0 and CoAl-2 were taken as samples to test the yields of CO and H₂ with the reaction time. As shown in Figure 8A, CO

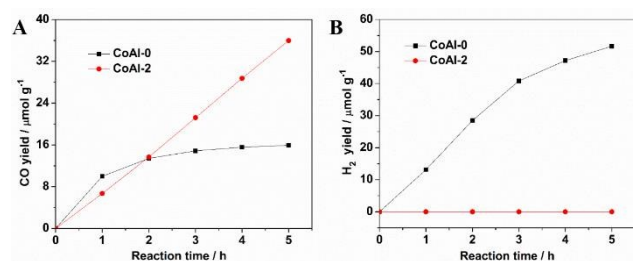
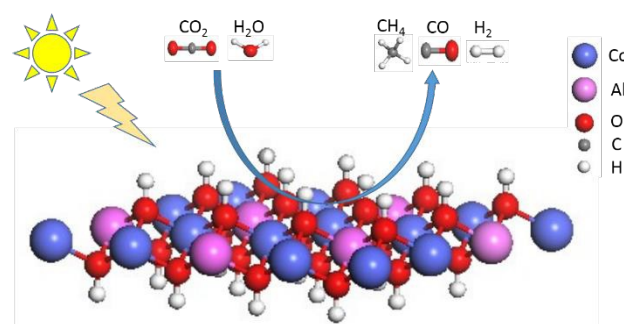


Figure 8. (A) Time course of CO evolution for CoAl-*n* (*n*=0, 2). (B) Time course of H₂ evolution for CoAl-*n* (*n*=0, 2).

emission for CoAl-0 gradually reached a platform with time, which has been exhibited in Figure S5. In comparison with CoAl-0, the CO emission for CoAl-2 increased steadily with reaction time. It is proposed that the decrease for CH₄ product could likely be in some connection with the sustaining CO emission, which was considered to be ascribed to the relative decrease of consumption rate compared with the production rate. Meanwhile, the H₂ emission for CoAl-*n* (*n*=0, 2) displayed distinct difference from each other (Figure 6B). The CoAl-0 exhibited relatively stable H₂ yield for the initial several hours, while little H₂ emission was detected using CoAl-2 as the photocatalyst. As is known, H in the CH₄ originates from the H in H₂O for CO₂ photoreduction with water. Hence, the activation of water to release H is of great significance for CH₄ formation. H₂ emission was experimentally observed for CoAl-0 catalyst, indicating that CoAl-0 must have the ability to dissociate water to release H, while CoAl-2 is likely to have negligible activity to dissociate water to release H for the further reaction with carbon intermediates like CO, which might account for the decrease of CO consumption rate and the sustaining increase of CO yield. It should be noted that the divalent cobalt is frequently-used element employed in water splitting by virtue of the unique and effective electronic structure configuration.⁴⁰⁻⁴² Therefore, it is proposed that the poor CH₄ yield of CoAl-2 could likely stem from the weak ability to dissociate water to release H when the divalent cobalt was oxidized. In addition, it has been demonstrated that Co (II) could convert into Co (I) under photo-excitation, and then the photoexcited electrons could be transferred to CO₂ from Co (I).⁴³ All above indicate the unique and effective property of the divalent cobalt for CO₂ photoreduction.

In addition to CoAl-LDHs, we further explored the CO₂ photoreduction activity of CoM-LDHs (M=Cr, Fe) and NAl-LDHs (N=Zn, Ni) synthesized by the same method as CoAl-LDHs. XRD patterns, UV-visible absorption spectra and FT-IR spectra of these LDHs were displayed in Figure S10, Figure S11, and Figure S12. The CH₄ formation rates for CoFe-LDHs and CoCr-LDHs were 2.2 μmol·g⁻¹·h⁻¹ and 3.3 μmol·g⁻¹·h⁻¹, respectively (Figure S13). CoM-LDHs (M=Cr, Fe) exhibited efficient activity for CO₂ photoreduction to CH₄ while there was little CH₄ yield for NAl-LDHs (N=Zn, Ni), possibly indicating the universality of the divalent cobalt for CO₂ photoreduction.

The mechanism of CO₂ photoreduction is complex, and CH₄ generation is considered to be a multi-step process. Generally,



Scheme 1. CO₂ photoreduction on CoAl-LDH nanosheets with water.

the first step to activate CO₂ over catalysts is of great significance for the subsequent reactions, since efficient binding could greatly reduce the high potential barrier and accelerate the dissociation of CO₂. CO₂ photoreduction over CoAl-LDHs is suggested to begin with the chemisorption between CO₂ and the OH groups. The linear CO₂ molecules become bent and activated after binding with surface OH Lewis bases, forming carbonate-like species. The carbonate-like species could then possibly be converted into CO accompanied by the break of C=O under illumination. Meanwhile, water is dissociated to proton and hydroxyl by the divalent cobalt. The adsorbed CO could likely be further converted into CH₄ via the proton-assisted multi-electron transfer mechanism while some H₂ was generated by direct combination of two protons and two electrons.

4. Conclusions

In summary, CoAl-LDH nanosheets were synthesized by a facile co-precipitation method and showed a hexagonal sheet-like morphology with a lateral size of about 80 nm and a thickness of about 18 nm. The CoAl-LDH nanosheets exhibited efficient catalytic activity and good stability for low-concentration CO₂ photoreduction to CH₄ with water under simulated solar light. The origins are considered to derive from the surface alkaline OH groups for efficient adsorption of low-concentration CO₂ and the divalent cobalt for dissociating water to release hydrogen for the hydrogenation process of the intermediate products. This work will help to shed light on the design of catalysts for low-concentration CO₂ photoreduction.

Acknowledgements

We acknowledge the financial support from the National Natural Science Foundation of China (51772312, 51472260).

Notes and references

- 1 A. M. Appel, J. E. Bercaw, A. B. Bocarsly, H. Dobbek, D. L. DuBois, M. Dupuis, J. G. Ferry, E. Fujita, R. Hille, P. J. Kenis, C. A. Kerfeld, R. H. Morris, C. H. Peden, A. R. Portis, S. W. Ragsdale, T. B. Rauchfuss, J. N. Reek, L. C. Seefeldt, R. K. Thauer and G. L. Waldrop, *Chem. Rev.*, 2013, **113**, 6621-6658.
- 2 X. Liu, S. Inagaki and J. Gong, *Angew. Chem. Int. Ed. Engl.*, 2016, **55**, 14924-14950.
- 3 X. Chang, T. Wang and J. Gong, *Energy Environ. Sci.*, 2016, **9**, 2177-2196.
- 4 X. Meng, S. Ouyang, T. Kako, P. Li, Q. Yu, T. Wang and J. Ye, *Chem. Commun.*, 2014, **50**, 11517-11519.
- 5 S. Xie, Y. Wang, Q. Zhang, W. Fan, W. Deng and Y. Wang, *Chem. Commun.*, 2013, **49**, 2451-2453.
- 6 M. Li, L. Zhang, M. Wu, Y. Du, X. Fan, M. Wang, L. Zhang, Q. Kong and J. Shi, *Nano Energy*, 2016, **19**, 145-155.
- 7 G. Xi, S. Ouyang, P. Li, J. Ye, Q. Ma, N. Su, H. Bai and C. Wang, *Angew. Chem. Int. Ed. Engl.*, 2012, **51**, 2395-2399.
- 8 J. Yu, J. Jin, B. Cheng and M. Jaroniec, *J. Mater. Chem. A*, 2014, **2**, 3407.
- 9 S. Wang, B. Y. Guan, Y. Lu and X. W. D. Lou, *J. Am. Chem. Soc.*, 2017, **139**, 17305-17308.
- 10 R. Kuriki, M. Yamamoto, K. Higuchi, Y. Yamamoto, M. Akatsuka, D. Lu, S. Yagi, T. Yoshida, O. Ishitani and K. Maeda, *Angew. Chem. Int. Ed.*, 2017, **129**, 4945-4949.
- 11 S. Wang, W. Yao, J. Lin, Z. Ding and X. Wang, *Angew. Chem. Int. Ed.*, 2014, **53**, 1034-1038.
- 12 G. Yang, D. Chen, H. Ding, J. Feng, J. Z. Zhang, Y. Zhu, S. Hamid and D. W. Bahnemann, *Appl. Catal. B: Environ.*, 2017, **219**, 611-618.
- 13 S. Wang and X. Wang, *Appl. Catal. B: Environ.*, 2015, **162**, 494-500.
- 14 R. Kuriki, H. Matsunaga, T. Nakashima, K. Wada, A. Yamakata, O. Ishitani and K. Maeda, *J. Am. Chem. Soc.*, 2016, **138**, 5159-5170.
- 15 S. Kumar, M. A. Isaacs, R. Trofimovaite, L. Durrndell, C. M. A. Parlett, R. E. Douthwaite, B. Coulson, M. C. R. Cockett, K. Wilson and A. F. Lee, *Appl. Catal. B: Environ.*, 2017, **209**, 394-404.
- 16 G. Chen, R. Gao, Y. Zhao, Z. Li, G. I. N. Waterhouse, R. Shi, J. Zhao, M. Zhang, L. Shang, G. Sheng, X. Zhang, X. Wen, L.-Z. Wu, C.-H. Tung and T. Zhang, *Adv. Mater.*, 2018, **30**, 1704663.
- 17 Y. Zhao, G. Chen, T. Bian, C. Zhou, G. I. Waterhouse, L. Z. Wu, C. H. Tung, L. J. Smith, D. O'Hare and T. Zhang, *Adv. Mater.*, 2015, **27**, 7824-7831.
- 18 C. G. Silva, Y. Bouzidi, V. Fornes and H. Garcia, *J. Am. Chem. Soc.*, 2009, **131**, 13833-13839.
- 19 B. Li, Y. Zhao, S. Zhang, W. Gao and M. Wei, *ACS. Appl. Mater. Inter.*, 2013, **5**, 10233-10239.
- 20 S. J. Kim, Y. Lee, D. K. Lee, J. W. Lee and J. K. Kang, *J. Mater. Chem. A*, 2014, **2**, 4136.
- 21 Y. Dou, S. Zhang, T. Pan, S. Xu, A. Zhou, M. Pu, H. Yan, J. Han, M. Wei, D. G. Evans and X. Duan, *Adv. Funct. Mater.*, 2015, **25**, 2243-2249.
- 22 G. Hu, N. Wang, D. O'Hare and J. Davis, *J. Mater. Chem.*, 2007, **17**, 2257.
- 23 Z. P. Liu, R. Z. Ma, M. Osada, N. Iyi, Y. Ebina, K. Takada and T. Sasaki, *J. Am. Chem. Soc.*, 2006, **128**, 4872-4880.
- 24 K. Parida, L. Mohapatra and N. Baliarsingh, *J. Phys. Chem. C*, 2012, **116**, 22417-22424.
- 25 J. Perez-Ramirez, G. Mul, F. Kapteijn and J. A. Moulijn, *J. Mater. Chem.*, 2001, **11**, 821-830.
- 26 O. Saber, *J. Mater. Sci.*, 2007, **42**, 9905-9912.
- 27 M. Al-Jaberi, S. Naille, M. Dossot and C. Ruby, *J. Mol. Struct.*, 2015, **1102**, 253-260.
- 28 S. Kumar, L. J. Durrndell, J. C. Manayil, M. A. Isaacs, C. M. A. Parlett, S. Karthikeyan, R. E. Douthwaite, B. Coulson, K. Wilson and A. F. Lee, *Part. Part. Syst. Character.*, 2017, **35**, 1700317.
- 29 Y. Matsumoto, *J. Solid State Chem.*, 1996, **126**, 227-234.
- 30 Y. Matsumoto, K. Sugiyama and E.-i. Sato, *J. Solid State Chem.*, 1988, **74**, 117-125.
- 31 K. L. Kauffman, J. T. Culp, A. Goodman and C. Matranga, *J. Phys. Chem. C*, 2011, **115**, 1857-1866.
- 32 A. Goodman, L. L. Campus, M. and K. Schroeder, T., *Energy & Fuels*, 2005, **19**, 471-476.
- 33 M. A. Ulibarri, J. M. Fernandez, F. M. Labajos and V. Rives, *Chem. Mater.*, 1991, **3**, 626-630.
- 34 A. Y. Khodakov, W. Chu and P. Fongarland, *Chem. Rev.*, 2007, **107**, 1692-1744.
- 35 B. J. Tan, K. J. Klabunde and P. M. A. Sherwood, *J. Am. Chem. Soc.*, 1991, **113**, 855-861.
- 36 W. Wei, W. Chen and D. G. Ivey, *Chem. Mater.*, 2008, **20**, 1941-1947.
- 37 S. Wang, Y. Hou, X. Wang, *ACS. Appl. Mater. Inter.*, 2015, **7**, 4327-4335.
- 38 M. Jiang, Y. Gao, Z. Wang and Z. Ding, *Appl. Catal. B: Environ.*, 2016, **198**, 180-188.
- 39 Y. Ji and Y. Luo, *ACS. Catal.*, 2016, **6**, 2018-2025.
- 40 M. W. Kanan and D. G. Nocera, *Science*, 2008, **321**, 1072-1075.

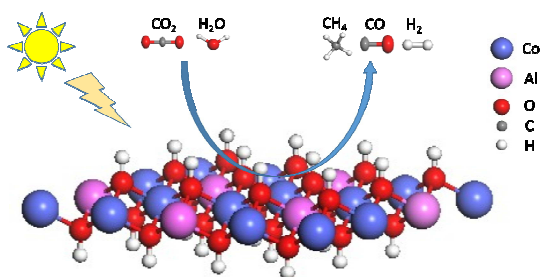
ARTICLE

Journal Name

- 41 W. Liu, L. Cao, W. Cheng, Y. Cao, X. Liu, W. Zhang, X. Mou, L. Jin, X. Zheng, W. Che, Q. Liu, T. Yao and S. Wei, *Angew. Chem. Int. Ed. Engl.*, 2017, **56**, 9312-9317.
- 42 L. Liao, Q. Zhang, Z. Su, Z. Zhao, Y. Wang, Y. Li, X. Lu, D. Wei, G. Feng, Q. Yu, X. Cai, J. Zhao, Z. Ren, H. Fang, F. Robles-Hernandez, S. Baldelli and J. Bao, *Nat. Nanotechnol.*, 2014, **9**, 69-73.
- 43 H. Zhang, J. Wei, J. Dong, G. Liu, L. Shi, P. An, G. Zhao, J. Kong, X. Wang, X. Meng, J. Zhang and J. Ye, *Angew. Chem. Int. Ed. Engl.*, 2016, **55**, 14310-14314.

View Article Online
DOI: 10.1039/C8TA01309H

Journal of Materials Chemistry A Accepted Manuscript

Graphical abstract

High CH₄ selectivity for CO₂ photoreduction of atmospheric concentration on CoAl-LDHs